

Article

Compositional Modeling of Impure CO₂ Injection for Enhanced Oil Recovery and CO₂ Storage

Hye-Seung Lee ¹, Jinhyung Cho ², Young-Woo Lee ¹ and Kun-Sang Lee ^{1,*}

¹ Department of Earth Resources and Environmental Engineering, Hanyang University, 222 Wangsimni-ro, Seongdong-gu, Seoul 04763, Korea; seung7185@hanyang.ac.kr (H.-S.L.); youngwoolee@hanyang.ac.kr (Y.-W.L.)

² Center for Climate, Environment Change Prediction Research, Ewha Womans University, 52 Ewhayeodae-gil, Seodaemun-gu, Seoul 03760, Korea; jh.cho@ewha.ac.kr

* Correspondence: kunslee@hanyang.ac.kr; Tel.: +82-222-202-240

Abstract: Injecting CO₂, a greenhouse gas, into the reservoir could be beneficial economically, by extracting remaining oil, and environmentally, by storing CO₂ in the reservoir. CO₂ captured from various sources always contains various impurities that affect the gas–oil system in the reservoir, changing oil productivity and CO₂ geological storage performance. Therefore, it is necessary to examine the effect of impurities on both enhanced oil recovery (EOR) and carbon capture and storage (CCS) performance. For Canada Weyburn W3 fluid, a 2D compositional simulation of water-alternating-gas (WAG) injection was conducted to analyze the effect of impure CO₂ on EOR and CCS performance. Most components in the CO₂ stream such as CH₄, H₂, N₂, O₂, and Ar can unfavorably increase the MMP between the oil and gas mixture, while H₂S decreased the MMP. MMP changed according to the type and concentration of impurity in the CO₂ stream. Impurities in the CO₂ stream also decreased both sweep efficiency and displacement efficiency, increased the IFT between gas and reservoir fluid, and hindered oil density reduction. The viscous gravity number increased by 59.6%, resulting in a decrease in vertical sweep efficiency. In the case of carbon storage, impurities decreased the performance of residual trapping by 4.1% and solubility trapping by 5.6% compared with pure CO₂ WAG. As a result, impurities in CO₂ reduced oil recovery by 9.2% and total CCS performance by 4.3%.

Keywords: CCUS; CO₂-EOR; carbon capture and storage; CCS-EOR; impure CO₂; water alternating gas (WAG)



Citation: Lee, H.-S.; Cho, J.; Lee, Y.-W.; Lee, K.-S. Compositional Modeling of Impure CO₂ Injection for Enhanced Oil Recovery and CO₂ Storage. *Appl. Sci.* **2021**, *11*, 7907. <https://doi.org/10.3390/app11177907>

Academic Editor: Fulvia Chiampo

Received: 3 August 2021

Accepted: 25 August 2021

Published: 27 August 2021

Publisher's Note: MDPI stays neutral with regard to jurisdictional claims in published maps and institutional affiliations.



Copyright: © 2021 by the authors. Licensee MDPI, Basel, Switzerland. This article is an open access article distributed under the terms and conditions of the Creative Commons Attribution (CC BY) license (<https://creativecommons.org/licenses/by/4.0/>).

1. Introduction

The CO₂-enhanced oil recovery (EOR) method has been widely applied to numerous field projects around the world [1,2]. CO₂-EOR was mostly aimed at recovering residual oil initially, but it is converted to not only increase recovery but also achieve reduction greenhouse gases by injecting CO₂ or flue gas. Recently, the application has been extended to unconventional hydrocarbons such as gas hydrates [3]. Existing CO₂-EOR aimed to produce maximum oil and inject minimum CO₂, but carbon capture, utilization, and storage (CCUS) consider the increase in oil recovery and greenhouse gas storage [4–6]. With atmospheric CO₂ concentrations continuing to rise worldwide, CCUS has the potential to reach net-zero [7]. As a key technology used to reduce carbon dioxide emissions from fossil-fueled power plants and other industrial activities, CCUS helps provide energy security by lowering emissions while achieving economics. CCUS is considered as an important technology for moving toward a global low-carbon economy. There are many sources of CO₂ such as natural gas reservoirs containing CO₂, industrial or anthropogenic sources, and natural CO₂ reservoirs. Depending on the capture approaches (post-combustion, oxy-fuel, or pre-combustion), various impurities such as N₂, O₂, H₂S, CH₄, Ar, and water are contained in the CO₂ stream [8–12]. The CO₂ concentration used for EOR commonly

requires extremely high purity (around 90–98%), especially for miscible displacement [13]. A purification process is generally required to obtain the appropriate CO₂ concentration from the source gas [14]. The purity of captured CO₂ largely depends on the type of capture technology. The type and amount of impurities in the CO₂ stream affect the fluid properties and thermodynamics of CO₂ differently, exhibiting beneficial or negative effects on CO₂-EOR: fluid solubility, phase behavior of the oil and gas system, and miscibility [15,16]. A small number of impurities significantly changes the physical properties and phase behavior of the CO₂ mixtures. The solubility in water depends on the type and amount of impurities in the CO₂ stream [17–19]. The solubility of CO₂ in water increases with increasing pressure and decreasing temperature. Most impurities have low solubility in water compared with CO₂. Impurities reduce the partial pressure of CO₂ and therefore reduce solubility in water. CO₂ impurities can affect all stages of CO₂-EOR, from CO₂ capture to flooding. Since the level of contaminant removal is determined by process technology and cost, the actual level of CO₂ purity required depends not only on the requirements of transportation and storage but also on the economics of the process. Separating impurities greatly increases the capture cost. Higher CO₂ purity is associated with higher costs of capture. The cost of a low purity CO₂ stream (82.9 wt.% CO₂) is 42% lower than high purity CO₂ (99.98 wt.% CO₂) in a capture plant [14]. It can be economical to inject the impurities contained in the CO₂ together. Several studies have investigated the effects of contaminants in the CO₂ stream on minimum miscibility pressure (MMP) to determine how impurities affect MMP compared with pure CO₂. In general, impurities including CH₄, SO₂, O₂, and N₂ have been found to increase MMP, while H₂S, C₂H₆, or intermediate hydrocarbons such as C₃ or C₄ reduce MMP, positively affecting miscible displacement [8,16,20–22]. Based on the effect of individual impurities on the phase behavior and MMP of the CO₂–hydrocarbon system, the effect of impurity mixtures on MMP and EOR performance has also been examined [16]. In addition, several studies have investigated the change of EOR performance and storage capacity when impurities and CO₂ are co-injected in the aquifer [10,11]. The presence of contaminants will affect the trapping mechanism since it changes the wettability, interfacial tension, and buoyancy of CO₂ [23,24]. However, studies on CO₂-EOR performance coupled with CO₂ storage considering the composition of the actual impure CO₂ stream from carbon sources are insufficient. Previous studies have focused on laboratory investigation, and discussions on reservoir-scale studies considering the composition of actual CO₂ are insufficient. Therefore, it is important to investigate the impact of impurities on CO₂ properties combined with the performance of EOR and carbon storage. In this study, compositional simulation was used to investigate the impact of impurities on the phase behavior of CO₂, CO₂ displacement mechanism, and carbon storage when injected without removing impurities from the oxy-fuel combustion stream.

2. Materials and Methods

2.1. Fluid Modeling

The Weyburn reservoir, located in southeast Saskatchewan, became a target for CO₂-EOR and carbon sequestration after water flooding production [25]. Since the reservoir has been conducting CO₂ monitoring and operated as a storage project, Weyburn W3 fluid data [25] is used to examine the interactions of reservoir fluid and CO₂ for the purpose of CCS-EOR. The composition of the reservoir oil and fluid properties used for the EOS calculations are summarized in Table 1 [26,27].

Regression was used to match the W3 fluid experimental measurements and fluid model data by tuning the EOS parameters. Table 2 shows PVT properties according to the dissolved gas mole fraction [25]. The properties are saturation pressure, gas oil ratio (GOR), gas solubility, formation volume factor (FVF), and swelling factor (SF). Fluid characterization, lumping of components, and matching with laboratory data are performed through regression using a modification of the adaptive least-squares algorithm of Dennis et al. [28]. The Peng–Robinson equation of state (PR-EOS) was used to construct the fluid model. Table 3 presents a comparison of experimental and simulation PVT properties of the fluid.

Through the regression method, results from the fluid model were properly matched to the experimental measurements and verified reliability.

Table 1. Oil composition and properties for equation of state (EOS) calculations.

Component	Composition	Critical Pressure (kPa)	Critical Temperature (K)	Molecular Weight (g/gmol)	Acentric Factor	Parachor
N ₂	0.0207	3394.4	126.2	28.0	0.04	41
CO ₂	0.0074	7376.5	304.2	44.0	0.23	78
H ₂ S	0.0012	8936.9	373.2	34.1	0.1	80
Methane, C ₁	0.0749	4600.2	190.6	16.0	0.01	77
Ethane, C ₂	0.0422	4883.9	305.4	30.1	0.1	108
Propane, C ₃	0.0785	4245.5	369.8	44.1	0.15	150
Butane, C ₄	0.0655	3722.7	416.5	58.1	0.19	186
Pentane, C ₅	0.0459	3379.4	464.9	72.1	0.24	228
C ₆₋₉	0.2156	3019.6	556.3	102.5	0.33	297
C ₁₀₋₁₇	0.2202	2017.5	692.2	184.0	0.58	508
C ₁₈₋₂₇	0.1027	1327.0	808.4	306.2	0.89	771
C ₂₈₊	0.1252	1155.1	915.5	566	1.1	1112

Table 2. PVT properties of the reservoir fluid and CO₂ mixtures at 140 °F.

Dissolved Gas Mole Fraction	Saturation Pressure (MPa)	GOR (sm ³ /m ³)	Gas Solubility (sm ³ /m ³)	FVF (m ³ /m ³)	SF (m ³ /m ³)
0.0058	2.9	19	0	1.087	1.074
0.158	4.5	42	23	1.143	1.13
0.412	8	113	94	1.308	1.292
0.439	8.4	125	106	1.336	1.32
0.521	9.9	158	139	1.409	1.392
0.595	11.4	221	202	1.546	1.527
0.641	12.6	263	244	1.634	1.614
0.826	19.7	875	856	2.694	2.668

Table 3. Comparison of the data for Weyburn fluid and the fluid model.

Parameters	W3	Fluid Model	Difference (%)
Oil density at saturation pressure (kg/m ³)	806.4	805.7	0.09
Saturation pressure (kPa)	4920	4916	0.08
Viscosity at saturation pressure (mPa·s)	1.76	1.76	0.0
Formation volume factor (m ³ /m ³)	1.12	1.108	1.07
API (°)	31	34.48	−11.23
MMP with CO ₂ (kPa)	14,196	13,900	2.09

2.2. Minimum Miscibility Pressure (MMP)

CO₂ is widely used in EOR through injection into an oil reservoir to increase oil recovery. CO₂ is used as a solvent, reducing oil viscosity and expanding the volume of oil in the reservoir. These phenomena can be expected to be more prominent if the oil and gas are more miscible. If the injected gas and fluid are not completely miscible, some of the gas does not dissolve into the oil and moves faster than the fluid, forming a separate phase. This causes an early breakthrough at the production well and lowers the productivity of the oil reservoir. To avoid this circumstance, determining whether the gas and fluid are under miscible conditions at the reservoir pressure is of significant interest. The lowest pressure to achieve miscibility by a multiple contact process under the given pressure and temperature is called the minimum miscibility pressure (MMP). Below the MMP, immiscible displacement occurs and consequently the oil recovery is reduced.

Methods for measuring MMP include the slim-tube test, the rising-bubble method, and the vanishing interfacial tension (VIT) test [29–33]. The slim-tube test has been widely used to measure MMP and is the most used method [34]. Since these methods are time-consuming, expensive, and sometimes less accurate, it is better to use the simulation method to determine the MMP. A slim-tube simulation model is conducted to measure the MMP. The slim tube is saturated with oil, and gas is subsequently injected to displace the oil in the slim tube. The amount of gas and oil is determined, and the recovery is defined. When the recovery is at least 90%, it is said that oil and gas are miscible. This process is repeated at different pressures, and the oil recovery is recorded at certain pressure. MMP from the slim-tube simulation is estimated as the lowest pressure with a recovery of 90% of the oil–gas system [35].

2.3. Evaluation of CO₂ Streams

CO₂ can be captured from various sources through various technologies, and impurities such as N₂, O₂, CH₄, H₂S, Ar, and water may exist in the CO₂ stream. The amounts of impurities contained in CO₂ depends on the degree of fuel oxidation and characteristics of the fuel. Among the three general CO₂ capture methods, pre-combustion, post-combustion, and oxy-fuel combustion, the oxy-fuel combustion process generates the highest impurities content in the CO₂ stream. Due to the use of lower purity oxygen, which is relatively cost-effective, significant amounts of air-derived impurities such as N₂, O₂, and Ar are produced. Table 4 presents the main impurities from different CO₂ capture technologies [13]. In this study, the composition of the gas obtained from the oxy-fuel scenario with the lowest CO₂ purity level was used to predict how many contaminants will affect performance and to compare the CO₂-EOR and CO₂ storage efficiency of impure and pure CO₂.

Table 4. Summary of CO₂ impurities from different CO₂ capture technologies.

	Oxy-Fuel Combustion			Pre-Combustion	Post-Combustion
	Raw/Dehumidified	Double Flashing	Distillation		
CO ₂ (% v/v)	74.8–85.0	95.84–96.7	99.3–99.4	95–99	99.6–99.8
O ₂ (% v/v)	3.21–6.0	1.05–1.2	0.01–0.4	0	0.015–0.0035
N ₂ (% v/v)	5.80–16.6	1.6–2.03	0.01–0.2	0.0195–1	0.045–0.29
Ar (% v/v)	2.3–4.47	0.4–0.61	0.01–0.1	0.0001–0.15	0.0011–0.021
NO _x (ppmv)	100–709	0–150	33–100	400	20–38.8
SO ₂ (ppmv)	50–800	0–4500	37–50	25	0–67.1
SO ₃ (ppmv)	20		20		
H ₂ O (ppmv)	100–1000	0	0–100	0.1–600	100–640
CO (ppmv)	50		50	0–2000	1.2–10
H ₂ S/COS (ppmv)				0.2–34,000	
H ₂ (ppmv)				20–30,000	
CH ₄ (ppmv)				0–112	

2.4. Solubility

A Solubility of gas in connate water is considered by including Henry's law as follows [36].

$$f_{iw} = y_{iw}H_i \quad (1)$$

where f_{iw} is the fugacity of the component i , y_{iw} is the composition of the component i in the aqueous phase and H_i is the Henry's law constant. The Henry's law constant can be expressed by [37]:

$$\ln H_i = \ln H_i^* + \frac{\bar{V}_i(p - p^*)}{RT} \quad (2)$$

where H_i^* is the Henry's law constant for component i at reference pressure, p^* is the reference pressure, \bar{V}_i is the partial molar volume of component i at infinite dilution, R is

the universal gas constant, and T is the temperature. The values are obtained from Li and Nghiem's method [36].

2.5. Reservoir Modeling

A compositional reservoir simulator, CMG-GEM, was used to simulate a two-dimensional (2D) vertical reservoir discretized into $52 \times 1 \times 20$ grid blocks of volume $3.048 \times 3.048 \times 1.524 \text{ m}^3$. The water-alternation-gas (WAG) injection scenario was used to investigate the miscibility and sweep efficiency with gravity override. In order to compare differences in the performance of EOR and CCS depending on the impurity content, the gas composition in Table 5 was used. The solubility of each component in water is considered by including Henry's law to represent gas solubility. Although impure gas was composed of 8 impurities, minor impurities at ppm levels such as H_2O , NO_x , SO_x , etc. were neglected. The injection process was conducted for 12 years, with water flooding in the first 2 years and WAG cycles of 10 years (Figure 1). During the 5 WAG cycles, water and gas were injected sequentially. Two injection cases were analyzed: 100% CO_2 + 0% impurities (Case 1) and 85% CO_2 + 15% impurities (Case 2) (Table 6). Each gas injection rate was constant at $566 \text{ ft}^3/\text{day}$ at surface condition. The initial reservoir condition is presented in Table 7. The producing bottom hole pressure was set to 2000 psi close to the MMP of 100% CO_2 , leading to miscible flooding in the case of pure CO_2 otherwise immiscible flooding in the case of impure CO_2 .

Table 5. Composition of CO_2 impurities from the low purity Oxy-fuel stream.

Components	Low Purity Level Oxy-Fuel Stream
CO_2 (vol%)	85.0
O_2 (vol%)	4.70
N_2 (vol%)	5.80
Ar (vol%)	4.47
H_2O (ppmv)	100
NO_x (ppmv)	100
SO_2 (ppmv)	50
SO_3 (ppmv)	20
CO (ppmv)	50

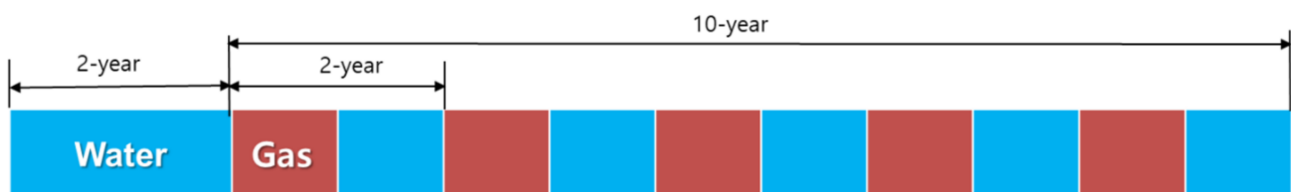


Figure 1. Water alternating gas (WAG) injection period.

Table 6. Classification of cases according to impurities content.

Case	Injection Gas Contents
1	100% CO_2 + 0% Impurities
2	75% CO_2 + 15% Impurities

Table 7. Reservoir initial and operating conditions.

Parameters	Values
Depth (ft)	4050
Initial reservoir pressure (psi)	4000
Reservoir temperature (°F)	145
Permeability in I, J, K-direction (md)	50, 50, 5
Porosity (%)	0.3
Initial oil saturation (%)	0.7
Initial water saturation (%)	0.3
Producing bottom hole pressure (psi)	2000

3. Results

3.1. Physical Properties of Impure Gas

MMP, Density, and Viscosity

A change in the physical properties of the gas will impact the displacement and sweep efficiencies. The slim-tube simulation method was conducted to determine CO₂ MMP for the reservoir fluid, which was matched against the experimental data. It has been recognized that MMP between the oil and injected solvents depends on the purity of CO₂. In general, the component of H₂S or intermediate hydrocarbons such as C₃, C₄ reduce the MMP, whereas the presence of N₂ and CH₄ in the CO₂ stream increase the MMP [38]. The MMP between CO₂ mixtures containing 10% of each representative impurity in the CO₂ such as CH₄, H₂, N₂, and O₂, and W3 fluid was calculated. The results from simulated MMPs using the slim-tube method with different mole fractions of CO₂ and impurities are shown in Table 8. Impurities of CH₄, H₂, N₂, and O₂ effected an increase in the MMP, while H₂S decreased the MMP. Therefore, CO₂ containing either components that increase (CH₄, H₂, N₂, O₂) or decrease (H₂S) MMP changes the miscibility.

Table 8. Minimum miscibility pressures (MMPs) calculation using the slim-tube method with various CO₂ mixtures.

Components	MMP (kPa)
CO ₂ 100%	13,900
CO ₂ 90% + CH ₄ 10%	18,616
CO ₂ 90% + H ₂ 10%	16,079
CO ₂ 90% + N ₂ 10%	18,933
CO ₂ 90% + O ₂ 10%	14,555
CO ₂ 90% + Ar 10%	18,650
CO ₂ 90% + H ₂ S 10%	12,714

Table 9 presents the impact of impure gas in the CO₂ on the gas properties. The MMP of pure CO₂ for this reservoir fluid was determined to be 13,900 kPa. Presence of the impure gas content increased the MMP to 19,927 kPa, while decreasing the density and viscosity, and had a negative impact on the miscibility of the gas and oil. The density of the injection gas impacted both injection rate and pressure. Density changes due to the addition of impurities reduced the gas compressibility and caused differences in bottomhole pressure at given injection wellhead pressure.

Table 9. Minimum miscibility pressures (MMPs) calculated using the slim-tube method with pure and impure CO₂ mixtures.

	Case 1	Case 2
Minimum Miscibility Pressure (kPa)	13,900	19,927
Density (kg/m ³)	689	552
Viscosity (mPa·s)	0.0702	0.0493

3.2. Effects of Impurities in CO₂ Streams on EOR Efficiency

3.2.1. Vertical Sweep Efficiency

The decrease in vertical sweep efficiency due to impurities in CO₂ is explained by the viscosity of the oil. Figure 2 shows the distribution of oil viscosity when 0.22 PV of gas is injected, indicating the decrease in vertical sweep efficiency due to impurities. In Case 2, impurities in the CO₂ stream cause the injected gas to move forward faster since it hinders the role of CO₂ in lowering the viscosity of oil. The blue swept area on the front represents the area where the injected fluid is in maximum contact with the oil, indicating the gas front. The minimum viscosity in Case 1 is 0.48 mPa·s and in Case 2 is 0.59 mPa·s. Therefore, the addition of 15% impurities generated a 22.9% decrease in the oil viscosity, indicating less gas acts as a solvent to decrease the oil viscosity after multiple contacts due to the impurities in CO₂.

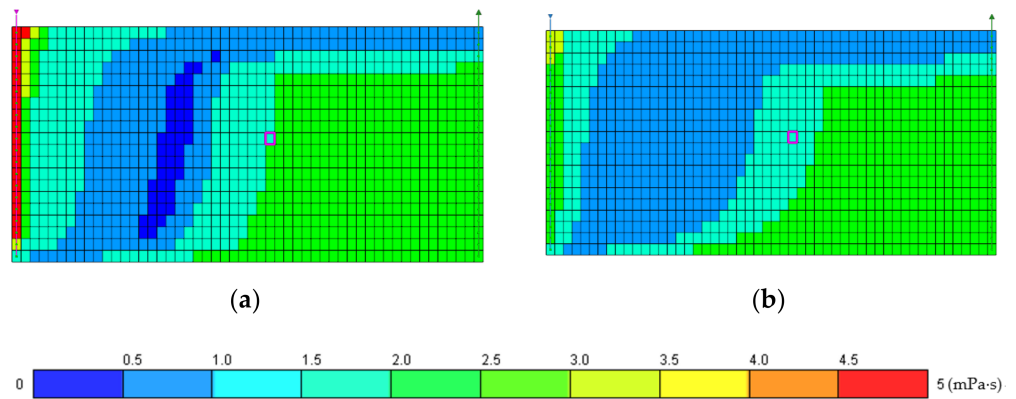


Figure 2. Oil viscosity distribution when 0.22 PV of gas is injected: (a) Case 1, (b) Case 2.

In horizontal gas flow through the cross-sectional 2D model, the vertical sweep efficiency was significantly reduced due to gravity segregation. The steeper the slope of the gas front of the sweep area, the more the injected gas contacts with the reservoir fluid. Since the difference in density and gravity between the injected fluid and reservoir fluid causes an override, the injected gas moves to the upper layer, reducing the vertical sweep efficiency. The change in vertical sweep efficiency due to the addition of impurities can be quantified by the viscous gravitational number (N_{gv}), which includes the terms of flooding velocity, density, and viscosity of fluid. The viscous gravitational can be expressed by [39]:

$$N_{gv} = \frac{\text{time for horizontal flow}}{\text{time for vertical flow}} = \frac{k_v k_{rs} \Delta \rho g \cos \alpha A L}{q_s \mu_s h} \quad (3)$$

where k_v is the vertical permeability, k_{rs} is the relative permeability, $\Delta \rho$ is the density difference between injected and reservoir fluids, g is the gravitational acceleration, A is the cross-sectional area, L is the length of the reservoir, q_s is the flow rate of the solvent, μ_s is the solvent viscosity, and h is the height of the reservoir. The range that determines whether gravity or viscous forces dominate is as follows [39]:

$$\begin{aligned} N_{gv} < 0.1 &: \text{Viscous forces dominate;} \\ 0.1 < N_{gv} < 10 &: \text{Intermediate;} \\ N_{gv} > 10 &: \text{Gravity dominates.} \end{aligned}$$

The decrease in vertical sweep efficiency was quantified from the viscous gravity number, as shown in Table 10. In Case 2, the viscous gravity number increased by as much as 59.6% by adding impurities into the CO₂. Since a larger viscous gravity number prevents the lower layer of the reservoir from being sufficiently swept, impurities in the injecting CO₂ stream lower the vertical sweep efficiency.

Table 10. Viscous gravity numbers of Cases 1 and 2.

Model	Viscous Gravity Number, N_{gv}
Case 1	2.1
Case 2	5.2

3.2.2. Displacement Efficiency

Above the MMP, the injected gas is completely mixed with the oil and the interfacial tension (IFT) between the injected gas and fluid would be negligible, affecting the relative permeability curves. The density and viscosity also decrease, leading to miscible displacement. The effect of adding impurities on the IFT between gas and oil in the grid block coordinates (12, 1 10) was investigated. The lowest IFT of Case 1 was 0.10 mN/m between the CO₂ and reservoir fluid, whereas for Case 2 it was 0.65 mN/m, a 547% higher value. The addition of impurities increased the IFT of Case 2 as shown in Figure 3, indicating that higher pressure would be required to achieve the miscible condition. In the same grid block of (12, 1, 10), the effect of reducing the density of oil was hindered as impurities were added to the CO₂ stream at the beginning of the injection period. After multiple contacts, Case 1 gave the lowest oil density value of 785 kg/m³ (2.5% reduction in initial oil density), while Case 2 gave a value of 799 kg/m³ (0.83% reduction in initial oil density). However, at some point, the oil density of Case 1 was greater than that of Case 2 since the intermediate and heavy components of the oil were displaced (Figure 4).

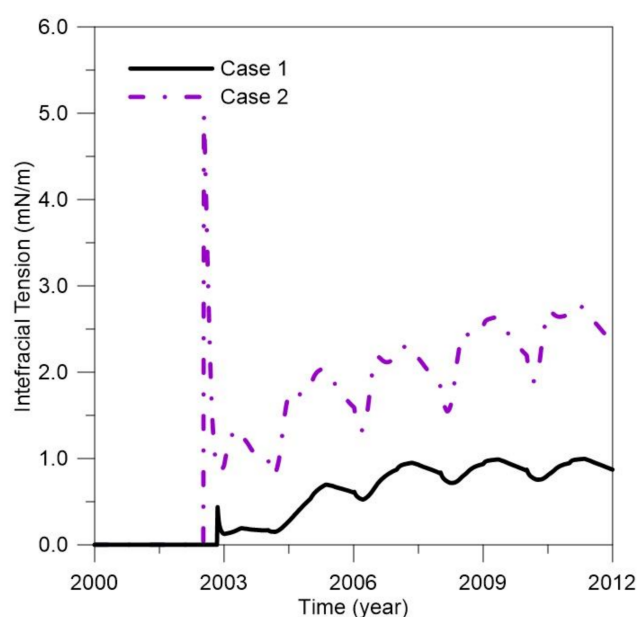


Figure 3. Interfacial tension between CO₂-impure gas and the oil during CO₂ and impure CO₂ WAG injection.

The cumulative gas injection under reservoir conditions obtained from CO₂ and impure CO₂ WAG is indicated in Figure 5. Impurities in the CO₂ stream have low critical temperatures and have relatively lower compressibility under the reservoir conditions [13]. CO₂ containing impurities would cause an increase in molar volume, i.e., impure CO₂ would occupy more volume than pure CO₂ under the same conditions. Although the injection rate was the same at the surface condition, the total amount of injected gas of Case 2 was greater than Case 1 under reservoir conditions. The gas moves faster in the upper layer in Case 2 than in Case 1, which causes an early gas breakthrough, as shown in Figure 5. This phenomenon occurs because the gas does not lower the viscosity of the oil compared with pure CO₂, and some of the injected gas forms a gas channel, causing early gas breakthrough in the production well, as shown in Figure 6.

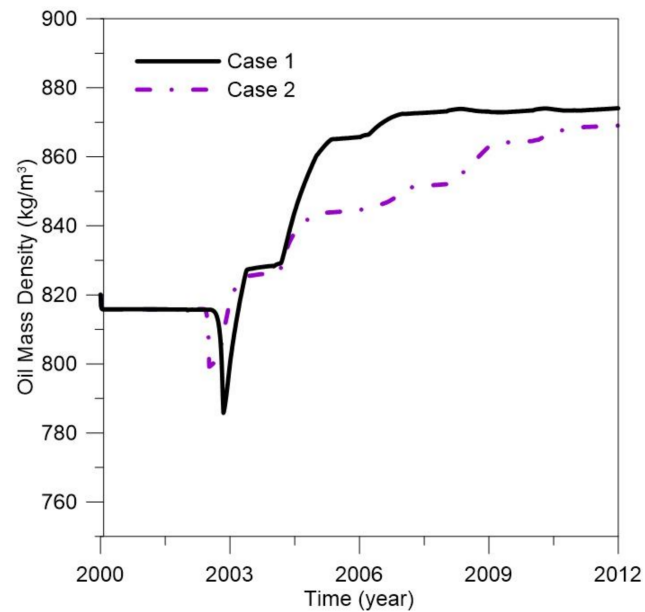


Figure 4. Oil density during CO₂ and impure CO₂ WAG injection.

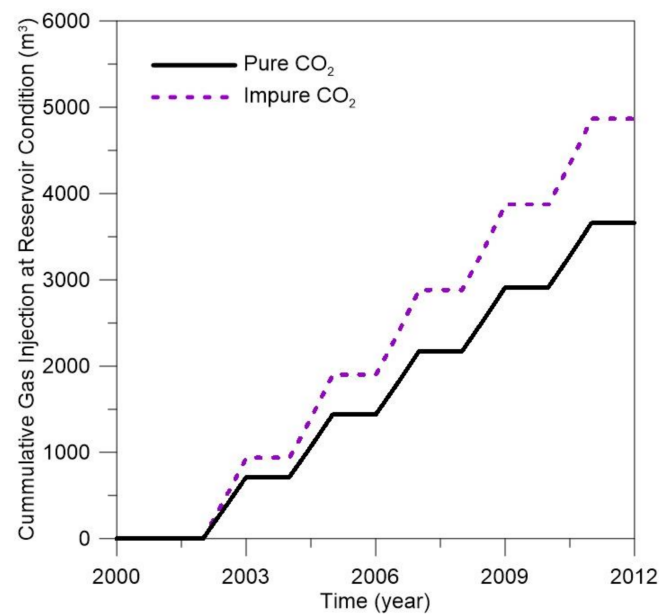


Figure 5. Cumulative gas injection during the CO₂ and impure CO₂ WAG injection under reservoir conditions.

The average reservoir pressure is presented in Figure 7. As the impurities are less compressible than CO₂, they occupy a larger volume in the pore, increasing the average reservoir pressure. However, due to significant reduction in the density of the injected stream caused by impurities, a higher flow pressure is required to achieve the same bottom hole pressure in the pure CO₂ case. Therefore, co-injection of impurities and CO₂ causes a relatively higher oil production compared with CO₂ injection at the early stage of WAG cycles. This trend is reversed due to the decrease in vertical sweep and displacing efficiency from the impurities, and the oil recovery is higher for Case 1 as shown in Figure 8. As a result, impurities in CO₂ reduce the oil recovery by 9.2%.

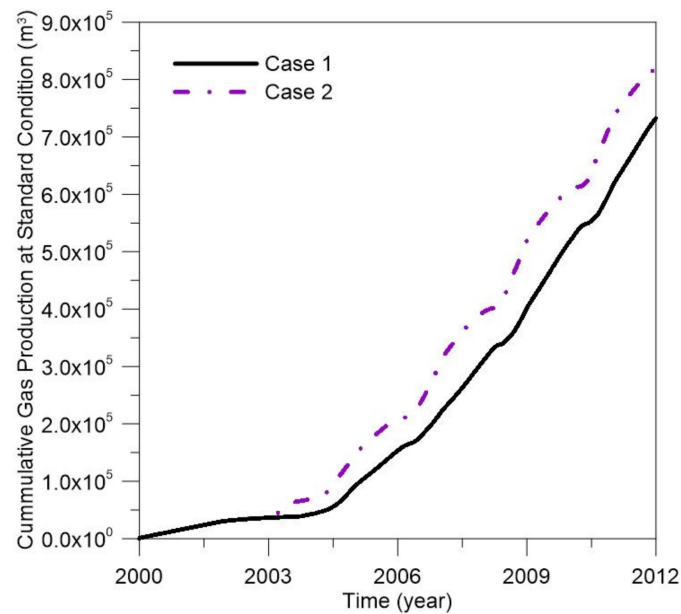


Figure 6. Cumulative gas production during the CO₂ and impure CO₂ WAG injection under standard conditions.

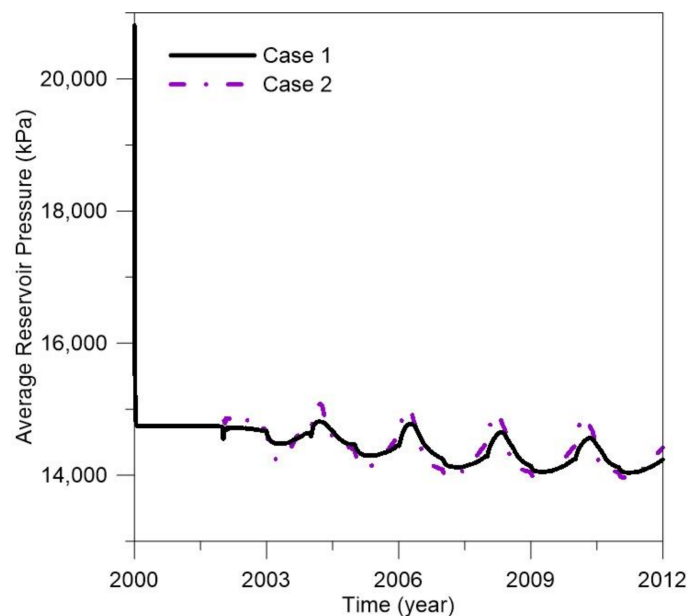


Figure 7. Average reservoir pressure during the CO₂ and impure CO₂ WAG injection.

3.3. Effects of Impurities in CO₂ Streams on Carbon Storage Efficiency

Figures 9 and 10 indicate the carbon sequestration by residual trapping and solubility trapping. Considering that impurities have less viscosity than CO₂, the presence of impurities increases the mobility and thus increases the horizontal movement of the injected gas. Since the density of impurities is lower than that of CO₂, the injected gas with impurities migrates upward easily. A significant volume of the injected gas moves and accumulates upward, which negatively affects residual trapping. Residually trapped CO₂ was reduced by 18.6% in Case 2 compared with Case 1. The solubility trapped CO₂ also decreased by 19.8% with the addition of impurities into CO₂. Since the absolute amount of injected CO₂ into the reservoir was less in Case 2 than in Case 1 due to the addition of impurities, the ratio of sequestered CO₂ to injected CO₂ was quantified. Figure 11 compares the ratio of

CO₂ stored by residual trapping and solubility trapping. In Case 2, the performance of residual trapping was reduced by 4.1% and solubility trapping by 5.6% compared with Case 1. As a result, impurities in CO₂ reduced the total CCS performance by 4.3%.

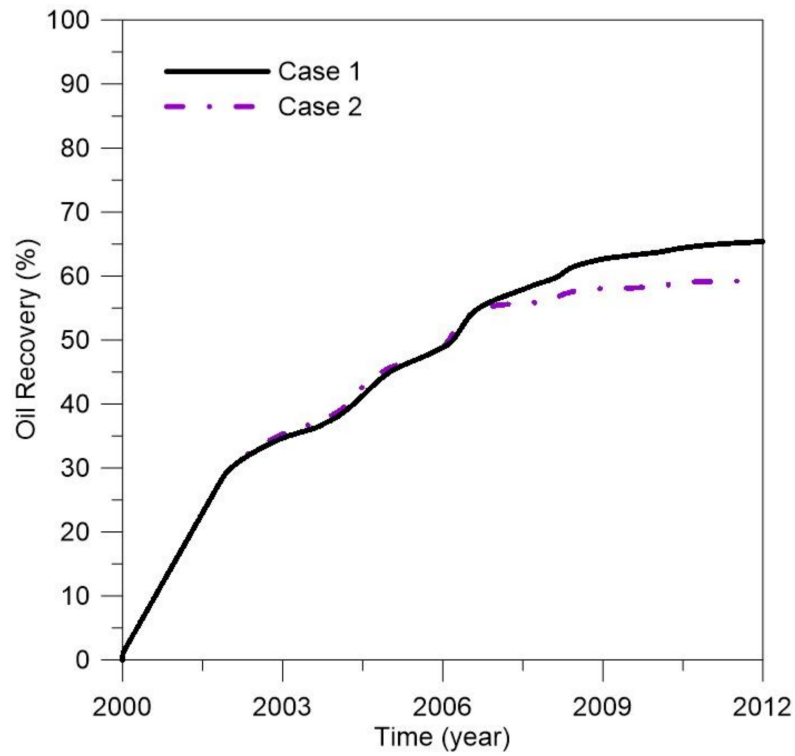


Figure 8. Oil recovery factor during the CO₂ and impure CO₂ WAG injection.

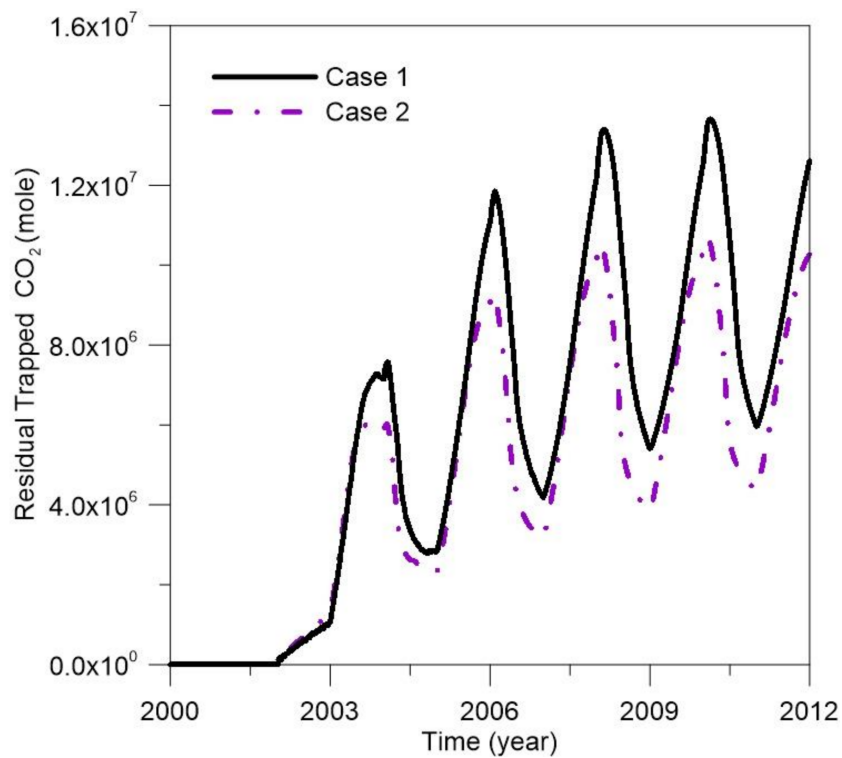


Figure 9. Residual CO₂ trapped by hysteresis during CO₂ and impure CO₂ WAG injection.

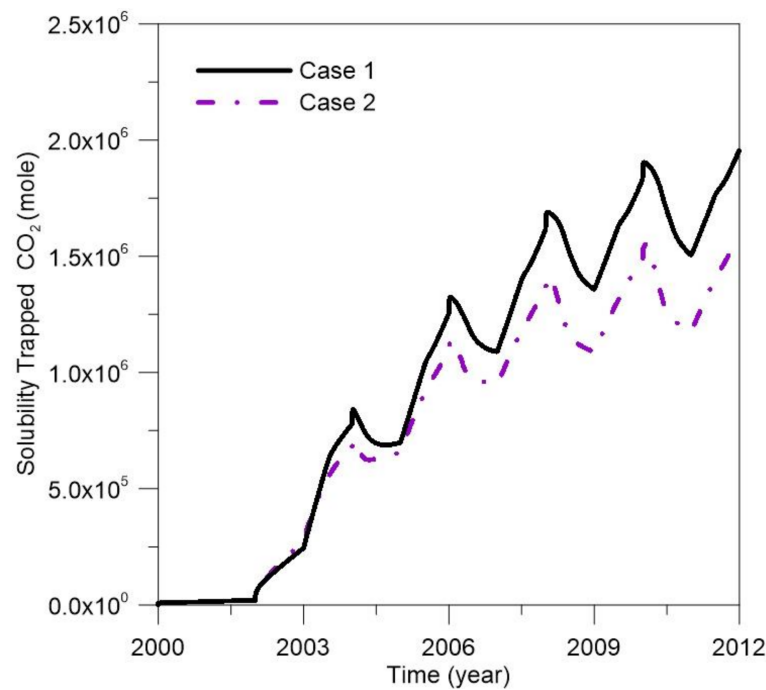


Figure 10. Solubility trapped CO₂ during CO₂ and impure CO₂ WAG injection.

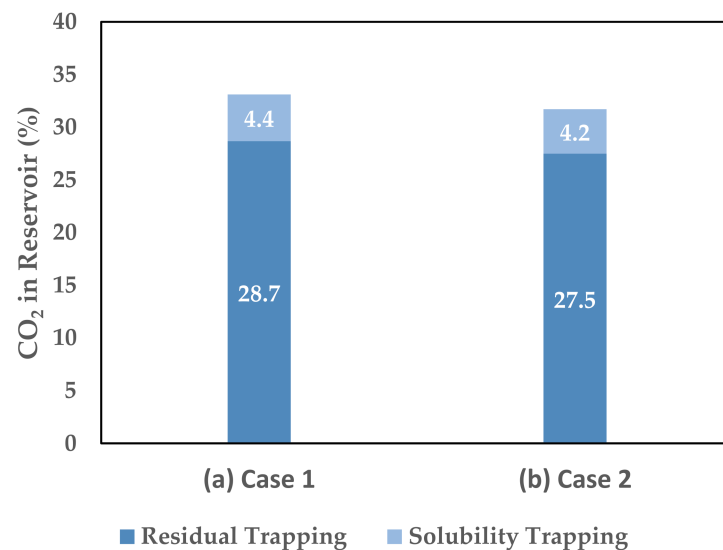


Figure 11. The comparison of trapping index: (a) Case 1, (b) Case 2.

4. Discussion

Impurities captured together with CO₂ are subjected to a purification process to generate high purity CO₂, which significantly increases the capture cost. Therefore, it is cost-effective to inject the CO₂ and impurities together. However, impure CO₂ adversely affects CO₂-EOR performance, resulting in reduced oil recovery. The change in oil recovery depending on the purity level would be controlled and considered. Though not considered in this study, it is important to develop the economic model to estimate the appropriate purity level of the CO₂ stream by using economic factors such as capital expenditures (CAPEX), operating expenditure (OPEX), tax credits, oil price, and CO₂ price depending on the purity level, sources and technology. For field applications, since the optimal operating conditions to increase the performance of CCS-EOR depend on the characteristics of the reservoir, it is necessary to develop a design for each site, such as different injection scenarios, based on economic analysis for field application.

5. Conclusions

This study aimed to investigate the effects of impurities in the CO₂ on CO₂-EOR and CCS performances. The degree of MMP change depended on the type of impurity since most non-condensable impurities increased the MMP, negatively affecting the miscible state except for H₂S. A compositional simulation was used to analyze the effect of impurities on both CO₂-EOR efficiency and carbon storage. A 2D vertical model was used to investigate vertical sweep efficiency considering gravity override during the WAG injection period. Two cases were analyzed: pure CO₂ (Case 1) and impure CO₂, with a composition of 15% impurities captured from oxy-fuel combustion (Case 2). The vertical sweep efficiency and displacement efficiency were affected by the impurities and eventually affected the oil recovery and CO₂-EOR performance. Impurities in the CO₂ stream increased the IFT and hindered the reduction in oil density. The viscous gravity number increased by 59.6%, confirming the decrease in vertical sweep efficiency due to the addition of impurities. The IFT on a specific grid block increased by 547% in Case 2. The effect of reducing oil density as a solvent was also inhibited from 2.5% to 0.83%. As a result, impurities in CO₂ reduced oil recovery by 9.2%. Due to CO₂ impurities, residual trapping performance was reduced by 4.1%, solubility trapping decreased by 5.6%, and the total CCS performance was reduced by 4.3%.

Author Contributions: Conceptualization, H.-S.L. and K.-S.L.; methodology, H.-S.L., J.C., Y.-W.L. and K.-S.L.; software, H.-S.L. and J.C.; validation, H.-S.L. and K.-S.L.; formal analysis, H.-S.L.; investigation, H.-S.L., J.C. and Y.-W.L.; resources, H.-S.L. and K.-S.L.; data curation, H.-S.L.; writing—original draft preparation, H.-S.L.; writing—review and editing, H.-S.L. and K.-S.L.; visualization, H.-S.L., J.C. and Y.-W.L.; supervision, K.-S.L.; project administration, K.-S.L.; funding acquisition, K.-S.L. All authors have read and agreed to the published version of the manuscript.

Funding: This work was supported by the National Research Foundation of Korea (NRF) grant funded by the Korea government (MSIT) (No. 2020R1F1A1070406). Jinhyung Cho was supported by a National Research Foundation of Korea (NRF) grant (No. 2020R111A1A01067015).

Institutional Review Board Statement: Not applicable.

Informed Consent Statement: Not applicable.

Data Availability Statement: The data presented in this study are available on request from the corresponding author.

Acknowledgments: The authors are grateful to the Computer Modelling Group Ltd. (CMG), Calgary, Canada for technical support.

Conflicts of Interest: The authors declare no conflict of interest.

References

1. Gozalpour, F.; Ren, S.R.; Tohidi, B. CO₂ EOR and storage in oil reservoir. *Oil Gas Sci. Technol.* **2005**, *60*, 537–546. [[CrossRef](#)]
2. Holm, L. Carbon dioxide solvent flooding for increased oil recovery. *Trans. AIME* **1959**, *216*, 225–231. [[CrossRef](#)]
3. Terzariol, M.; Goldsztein, G.; Santamarina, J.C. Maximum recoverable gas from hydrate bearing sediments by depressurization. *Energy* **2017**, *141*, 1622–1628. [[CrossRef](#)]
4. Kuuskraa, V.A.; Godec, M.L.; Dipietro, P. CO₂ utilization from “next generation” CO₂ enhanced oil recovery technology. *Energy Procedia* **2013**, *37*, 6854–6866. [[CrossRef](#)]
5. IEAGHG. *CO₂ Storage in Depleted Oilfields: Global Application Criteria for Carbon Dioxide Enhanced Oil Recovery*; IEAGHG Publications: Cheltenham, UK, 2009.
6. Khelifa, T.; Maini, B.B. Evaluation of CO₂ based vapex process for the recovery of bitumen from tar sand reservoirs. In Proceedings of the SPE International Improved Oil Recovery Conference in Asia Pacific, Kuala Lumpur, Malaysia, 20–21 October 2003.
7. Hassanpouryouzband, A.; Joonaki, E.; Edlmann, K.; Haszeldine, R.S. Offshore geological storage of hydrogen: Is this our best option to achieve net-zero? *ACS Energy Lett.* **2021**, *6*, 2181–2186. [[CrossRef](#)]
8. Choubineh, A.; Helalizadeh, A.; Wood, D.A. The impacts of gas impurities on the minimum miscibility pressure of injected CO₂-rich gas–crude oil systems and enhanced oil recovery potential. *Pet. Sci.* **2019**, *16*, 117–126. [[CrossRef](#)]
9. Chapoy, A.; Burgass, R.; Tohidi, B.; Austell, J.M.; Eickhoff, C. Effect of common impurities on the phase behavior of carbon-dioxide-rich systems: Minimizing the risk of hydrate formation and two-phase flow. *SPE J.* **2011**, *16*, 921–930. [[CrossRef](#)]

10. Chapoy, A.; Nazeri, M.; Kapateh, M.; Burgass, R.; Coquelet, C.; Tohidi, B. Effect of impurities on thermophysical properties and phase behaviour of a CO₂-rich system in CCS. *Int. J. Greenh. Gas Control* **2013**, *19*, 92–100. [[CrossRef](#)]
11. Jin, L.; Pekot, L.J.; Hawthorne, S.B.; Salako, O.; Peterson, K.J.; Bosshart, N.W.; Jiang, T.; Hamling, J.A.; Gorecki, C.D. Evaluation of recycle gas injection on CO₂ enhanced oil recovery and associated storage performance. *Int. J. Greenh. Gas Control* **2018**, *75*, 151–161. [[CrossRef](#)]
12. Ziabakhsh-Ganji, Z.; Kooi, H. An equation of state for thermodynamic equilibrium of gas mixtures and brines to allow simulation of the effects of impurities in subsurface CO₂ storage. *Int. J. Greenh. Gas Control* **2012**, *11*, S21–S34. [[CrossRef](#)]
13. IEAGHG. *Effects of Impurities on Geological Storage of CO₂*; IEAGHG Publications: Cheltenham, UK, 2011.
14. Kolster, C.; Mechleri, E.; Krevor, S.; Mac Dowell, N. The role of CO₂ purification and transport networks in carbon capture and storage cost reduction. *Int. J. Greenh. Gas Control* **2017**, *58*, 127–141. [[CrossRef](#)]
15. Bachu, S.; Bennion, D.B. Chromatographic partitioning of impurities contained in a CO₂ stream injected into a deep saline aquifer: Part 1. Effects of gas composition and in situ conditions. *Int. J. Greenh. Gas Control* **2009**, *3*, 458–467. [[CrossRef](#)]
16. Wilkinson, J.R.; Leahy-Dios, A.; Teletzke, G.F.; Dickson, J.L. Use of CO₂ containing impurities for miscible enhanced oil recovery. In Proceedings of the International Oil and Gas Conference and Exhibition in China, Beijing, China, 8–10 June 2010.
17. Savary, V.; Berger, G.; Dubois, M.; Lachapagne, J.; Pages, A.; Thibeau, S.; Lescanne, M. The solubility of CO₂ + H₂S mixtures in water and 2 M NaCl at 120 °C and pressures up to 35 MPa. *Int. J. Greenh. Gas Control* **2012**, *10*, 123–133. [[CrossRef](#)]
18. Shabani, B.; Vilcáez, J. Prediction of CO₂-CH₄-H₂S-N₂ gas mixtures solubility in brine using a non-iterative fugacity-activity model relevant to CO₂-MEOR. *J. Pet. Sci. Eng.* **2017**, *150*, 162–179. [[CrossRef](#)]
19. Dhima, A.; de Hemptinne, J.; Jose, J. Solubility of hydrocarbons and CO₂ mixtures in water under high pressure. *Ind. Eng. Chem. Res.* **1999**, *38*, 3144–3161. [[CrossRef](#)]
20. Zhang, P.Y.; Huang, S.; Sayegh, S.; Zhou, X.L. Effect of CO₂ impurities on gas-injection EOR processes. In Proceedings of the SPE/DOE Symposium on Improved Oil Recovery, Tulsa, OK, USA, 17–21 April 2004.
21. Luo, E.; Hu, Y.; Wang, J.; Fan, Z.; Hou, Q.; Ma, L.; Dai, S. The effect of impurity on miscible CO₂ displacement mechanism. *Oil Gas Sci. Technol.—Revue d'IFP Energ. Nouv.* **2019**, *74*, 1–20. [[CrossRef](#)]
22. Sayegh, S.; Huang, S.; Zhang, Y.; Lavoie, R. Effect of H₂S and pressure depletion on the CO₂ MMP of Zama Oils. *J. Can. Pet. Technol.* **2007**, *46*, 34–41. [[CrossRef](#)]
23. Blanco, S.T.; Rivas, C.; Fernández, J.; Artal, M.; Velasco, I. Influence of methane in CO₂ transport and storage for CCS technology. *Environ. Sci. Technol.* **2012**, *46*, 13016–13023. [[CrossRef](#)]
24. Ren, Q.; Chen, G.; Yan, W.; Guo, T. Interfacial tension of (CO₂+ CH₄)+ water from 298 K to 373 K and pressures up to 30 MPa. *J. Chem. Eng. Data* **2000**, *45*, 610–612. [[CrossRef](#)]
25. Srivastava, R.K.; Huang, S.S.; Dong, M. Laboratory investigation of Weyburn CO₂ miscible flooding. *J. Can. Pet. Technol.* **2000**, *39*, 41–51. [[CrossRef](#)]
26. Peng, D.Y.; Robinson, D.B. A new two-constant equation of state. *Ind. Eng. Chem. Fundam.* **1976**, *15*, 59–64. [[CrossRef](#)]
27. Robinson, D.B.; Peng, D.-Y. *The Characterization of the Heptanes and Heavier Fractions for the GPA Peng-Robinson Programs*; Research Report 28; Gas Processors Association: Tulsa, OK, USA, 1978.
28. Dennis Jr, J.E.; Gay, D.M.; Walsh, R.E. An adaptive nonlinear least-squares algorithm. *ACM Trans. Math. Softw. (TOMS)* **1981**, *7*, 348–368. [[CrossRef](#)]
29. Yellig, W.F.; Metcalfe, R.S. Determination and prediction of CO₂ minimum miscibility pressures (includes associated paper 8876). *J. Pet. Technol.* **1980**, *32*, 160–168. [[CrossRef](#)]
30. Elsharkawy, A.M.; Poettmann, F.H.; Christiansen, R.L. Measuring CO₂ minimum miscibility pressures: Slim-tube or rising-bubble method? *Energy Fuels* **1996**, *10*, 443–449. [[CrossRef](#)]
31. Dong, M.; Huang, S.; Dyer, S.B.; Mourits, F.M. A comparison of CO₂ minimum miscibility pressure determinations for Weyburn crude oil. *J. Pet. Sci. Eng.* **2001**, *31*, 13–22. [[CrossRef](#)]
32. Ayirala, S.C.; Rao, D.N. Comparative evaluation of a new gas/oil miscibility-determination technique. *J. Can. Pet. Technol.* **2011**, *50*, 71–81. [[CrossRef](#)]
33. Zhang, K.; Gu, Y. Two different technical criteria for determining the minimum miscibility pressures (MMPs) from the slim-tube and coreflood tests. *Fuel* **2015**, *161*, 146–156. [[CrossRef](#)]
34. Ahmad, W.; Vakili-Nezhaad, G.; Al-Bemani, A.S.; Al-Wahaibi, Y. Uniqueness, repeatability analysis and comparative evaluation of experimentally determined MMPs. *J. Pet. Sci. Eng.* **2016**, *147*, 218–227. [[CrossRef](#)]
35. Vulin, D.; Gaćina, M.; Biličić, V. Slim-tube simulation model for CO₂ injection EOR. *Rudarsko-Geološko-Naftni Zbornik* **2018**, *33*, 37–49. [[CrossRef](#)]
36. Li, Y.K.; Nghiem, L.X. Phase equilibria of oil, gas and water/brine mixtures from a cubic equation of state and Henry's law. *Can. J. Chem. Eng.* **1986**, *64*, 486–496. [[CrossRef](#)]
37. Stumm, W.; Morgan, J.J. *Aquatic Chemistry: Chemical Equilibria and Rates in Natural Waters*; John Wiley & Sons: Hoboken, NJ, USA, 2012; Volume 126.
38. Lake, L.W. *Enhanced Oil Recovery*; Prentice-Hall: Hoboken, NJ, USA, 1989.
39. Chugh, S.; Baker, R.; Cooper, L.; Spence, S. Simulation of horizontal wells to mitigate miscible solvent gravity override in the Virginia Hills Margin. *J. Can. Pet. Technol.* **2000**, *39*, 28–34. [[CrossRef](#)]